Mon. Not. R. Astron. Soc. **000**, 000–000 (0000) Printed 24 August 2007 (MN LATEX style file v2.2)

The Importance of Mergers for the Origin of Intracluster Stars in Cosmological Simulations of Galaxy Clusters

Giuseppe Murante[1,2], Martina Giovalli[3], Ortwin Gerhard[4], Magda Arnaboldi[1,5], Stefano Borgani[2,6,7], Klaus Dolag[8]

[1] *INAF, Osservatorio Astronomico di Torino, Strada Osservatorio 20, I-10025 Pino Torinese (Italy) (murante@to.astro.it)*
[2] *Dipartimento di Astronomia dell'Universitá di Trieste, Via Tiepolo 11, I-34131 Trieste (Italy)*
[3] *Dipartimento di Fisica Generale "Amedeo Avogadro", Universitádegli Studi di Torino, Torino (Italy) (giovalli@to.astro.it)*
[4] *Max-Planck-Institut für Extraterrestrische Physik, Giessenbachstrasse, Garching bei München, D-85741. Germany (gerhard@exgal.mpe.mpg.de)*
[5] *ESO - Karl-Schwarzschild-Str. 2D-85748 Garching bei München (arnaboldi@to.astro.it)*
[6] *INAF, Osservatorio Astronomico di Trieste, Via Tiepolo 11, I-34131 Trieste (Italy) (borgani@ts.astro.it)*
[7] *INFN, National Institute for Nuclear Physics, Trieste (Italy)*
[8] *Max-Planck-Institut für Astrophysik, Karl-Schwarzschild-Strasse, Garching bei München, D-85741. Germany (kdolag@mpa-garching.mpg.de)*

24 August 2007

ABSTRACT

We study the origin of the diffuse stellar component (DSC) in 117 galaxy clusters extracted from a cosmological hydrodynamical simulation. We identify all galaxies present in the simulated clusters at 17 output redshifts, starting with $z = 3.5$, and then build the family trees for all the $z = 0$ cluster galaxies. The most massive cluster galaxies show complex family trees, resembling the merger trees of dark matter halos, while the majority of other cluster galaxies experience only one or two major mergers during their entire life history. Then for each diffuse star particle identified at $z = 0$, we look for the galaxy to which it once belonged at an earlier redshift, thus linking the presence of the diffuse stellar component to the galaxy formation history.

The main results of our analysis are: (i) On average, half of the DSC star particles comes from galaxies associated with the family tree of the most massive galaxy (BCG), one quarter comes from the family trees of other massive galaxies, and the remaining quarter from dissolved galaxies. I.e., the formation of the DSC is parallel to the build-up of the BCG and other massive galaxies. (ii) Most DSC star particles become unbound during mergers in the formation history of the BGCs and of other massive galaxies, independent of cluster mass. Our results suggest that the tidal stripping mechanism is responsible only for a minor fraction of the DSC. (iii) At cluster radii larger than 250 h^{-1} kpc, the DSC fraction from the BCG is reduced and the largest contribution comes from the other massive galaxies; in the cluster outskirts, galaxies of all masses contribute to the DSC. (iv) The DSC does not have a preferred redshift of formation: however, most DSC stars are unbound at $z < 1$. (v) The amount of DSC stars at $z = 0$ does not correlate strongly with the global dynamical history of clusters, and increases weakly with cluster mass.

Key words: Galaxies: Clusters: General, Galaxies: Elliptical and Lenticular, cD, Galaxies: Evolution

1 INTRODUCTION

Observations of diffuse intracluster light and individual intracluster stars in nearby clusters (Arnaboldi et al. 2002, 2003, 2004; Feldmeier et al. 2003; Mihos et al. 2005; Gerhard et al. 2005) and at intermediate redshift (Gonzalez et al. 2000; Feldmeier et al. 2004; Zibetti et al. 2005) indicate that a substantial fraction of stars becomes unbound from galaxies as these fall towards the densest parts of their cluster environment.

The radial distribution of the intracluster light (ICL) in galaxy clusters is observed to be more centrally concentrated than that of the cluster galaxies (Zibetti et al. 2005), a result which was predicted from cosmological hydrodynamical simulations of galaxy clusters (Murante et al. 2004, M04 hereafter). Zibetti et al. (2005) also find that the surface brightness of the ICL correlates both with

BCG luminosity and with cluster richness, while the fraction of the total light in the ICL is almost independent of these quantities. Other observations indicate an increase of the relative fraction of diffuse stars from the mass scale of loose groups (less than 2 %, Castro-Rodríguez et al. (2003), Feldmeier et al. (2003)) to that of Virgo-like clusters (Feldmeier et al. 2003; Arnaboldi et al. 2003; Mihos et al. 2005, $\approx 5-10\%$) up to the most massive clusters (Gonzalez et al. 2000; Feldmeier et al. 2002; Gal-Yam et al. 2003; Feldmeier et al. 2004; Krick et al. 2006, 10-20 % or higher).

The origin and evolution of this diffuse stellar component (DSC) is currently unknown and several mechanism are being investigated. The ICL may be produced by stripping and disruption of galaxies as they pass through the central regions of relaxed clusters (Byrd & Valtonen 1990; Gnedin 2003). Other mechanisms are the stripping of stars from galaxies during the initial formation of clusters (Merritt 1984); creation of stellar halos in galaxy groups, that later fall into massive clusters, and then become unbound (Mihos 2004; Rudick et al. 2006); stripping of stars during high–speed galaxy encounters in the cluster environment (Moore et al. 1996). Evidence for ongoing stripping from elliptical galaxies in clusters was presented by Cypriano et al. (2006).

In parallel, numerical simulations have been performed to investigate the properties the DSC in galaxy clusters within the current cosmological models. Napolitano et al. (2003) used Dark-Matter (DM) only simulations, and identified the stellar component using the DM particles as tracers. For the first time, M04 used a ΛCDM cosmological hydrodynamical simulation, including radiative cooling and star formation, to quantify the amount and the distribution of the DSC in a set of 117 clusters. Willman et al. (2004) and Sommer-Larsen et al. (2005) found a DSC in their simulated single clusters. Willman et al. (2004) discussed the origin of the DSC: they found a correlation between the cluster growth and the increase in the DSC mass, and that both massive and small galaxies contribute to its formation.

Recently, Rudick et al. (2006) performed collisionless simulations where high–resolution model galaxies were inserted in their dark matter halos at a given redshift, and then their common evolution in a cluster was followed from that time on. A DSC was formed, and Rudick et al. (2006) found that the cluster DSC grows with the accretion of groups during the cluster history.

In this work, we focus on the formation mechanism of the ICL in a cosmological hydrodynamical simulation (Borgani et al. 2004, M04). The formation of galaxies and their subsequent dynamical evolution in a time dependent gravitational potential is a direct consequence of the hierarchical assembly process of cosmic structures. Using a large ($192^3 h^{-3}$ Mpc^3) volume simulation, we study a statistically significant ensemble of galaxy clusters and follow how stars become unbound from galaxies during the evolution of clusters as a function of cosmic time. We also address the stability of our results against numerical resolution by carrying out the same analysis on three clusters from this set, which were re-simulated at a substantially improved force and mass resolution.

The plan of the paper is as follows: in Section 2 we describe our numerical simulations and in Section 3 we give details on the galaxy identification and properties. In Section 4 we describe the identification of the diffuse stellar component (DSC). In Section 5 we present the link between galaxy histories and the formation of the DSC; in Section 6 we discuss how resolution and other numerical effect may affect our results; in Section 7 we discuss the dynamical mechanisms that unbind stars from galaxies in clusters and compare with the statistical analysis of the cosmological simulation performed in the previous Sections. In Section 8 we summarise our results and give our conclusions.

2 THE SIMULATED CLUSTERS

The clusters analysed in this paper are extracted from the large hydrodynamical simulation (LSCS) of a "concordance" ΛCDM cosmological model ($\Omega_m = 0.3$, $\Omega_\Lambda = 0.7$, $\Omega_{\rm b} = 0.019\,h^{-2}$, $h = 0.7$ and $\sigma_8 = 0.8$). This simulation is presented in Borgani et al. (2004) and we refer to that paper for additional details. The LSCS is carried out with the massively parallel Tree+SPH code GADGET2 (Springel et al. 2001; Springel 2005), and follows 480^3 dark matter particles and as many gas particles in a periodic box of size $192\,h^{-1}$ Mpc. Accordingly, the mass resolution is $m_{\rm dm} = 4.6 \times 10^9\,h^{-1} M_\odot$, $m_{\rm gas} = 6.9 \times 10^8 h^{-1} M_\odot$ and $m_{\rm star} = 3.465 \times 10^8 h^{-1} M_\odot$. The Plummer–equivalent softening length for the gravitational force is set to $\epsilon = 7.5\,h^{-1}$ kpc, fixed in physical units from $z = 0$ to $z = 2$, while being fixed in co-moving units at higher redshift. The SPH softening length of the gas is allowed to shrink to half the value of the gravitational force softening. The simulation includes radiative cooling, the effect of a photo–ionising uniform UV background, star formation using a sub-resolution multi-phase model for the interstellar medium (Springel & Hernquist 2003), feedback from supernovae (SN) explosions, including the effect of galactic outflows. The velocity of these galactic winds is fixed to $v_w \simeq 340\,{\rm km\,s^{-1}}$, which corresponds to 50% efficiency for SN to power the outflows.

Clusters are identified at $z = 0$ using a standard friends-of-friends (FOF) algorithm, with a linking length of 0.15 times the mean dark matter inter-particle separation. We identify 117 clusters in the simulation with $M_{FOF} > 10^{14} h^{-1} M_\odot$. Cluster centres are placed at the position of the DM particle having the minimum value of the gravitational potential. For each cluster, the virial mass $M_{\rm vir}$ is defined as the mass contained within a radius encompassing an average density equal to the virial density, $\rho_{\rm vir}$, predicted by the top–hat spherical collapse model. For the assumed cosmology, $\rho_{\rm vir} \simeq 100 \rho_c$, where ρ_c is the critical cosmic density (Eke et al. 1996, e.g.).

To test the effects of numerical resolution on the final results, we select three clusters, having virial masses $M_{\rm vir} = 1.6, 2.5, 2.9 \times 10^{14} h^{-1} {\rm M}_\odot$, and re-simulate them twice with different resolution. While the first, lower-resolution simulation is carried out at the same resolution as the parent simulation, the second simulation had a mass resolution $45\times$ higher, with a correspondingly smaller softening parameter, $\epsilon = 2.1\,h^{-1}$ kpc. These re-simulations are performed using more efficient SN feedback, with a wind velocity $v_w \simeq 480\,{\rm km\,s^{-1}}$. A detailed description of these re–simulations is provided by Borgani et al. (2006).

3 IDENTIFYING GALAXIES IN A CLUSTER WITH SKID

The identification of substructures inside halos is a longstanding problem, which is not uniquely solved. In the present work, we need to identify galaxies in the simulations from the distribution of star particles which fill the volume of the cosmological simulation.

In the LSCS, "galaxies" are defined as self—bound, locally over-dense structures, following the procedure in M04, which is

based on the publicly available SKID algorithm[1] (Stadel 2001). At a given redshift, once the star particles have been grouped by SKID, we classify as galaxies only those groups which contain at least 32 bound star particles. There is a degree of uncertainty in the galaxy identification by SKID, as in other similar identification algorithms, which comes in from the assignment of those star particles which are located in its outskirts of each self-bound object. The main advantage of this identification algorithm is that it provides a dynamically–based, automated, operational way to decide whether a star particle belongs to a gravitationally bound object or not. Additional details of the galaxy identification algorithm and on our tests are given in the Appendix.

We expect that, once a self-bound structure of luminous particles has been formed at a given redshift, most of its mass will remain in bound structures, for all subsequent redshifts. However, it may happen that a group of particles classified as a "galaxy" at one output redshift, with a number of particles just above the specified minimum particle threshold for structure identification, may fall below this limit at the next redshift output. This may occur, for example, because the group is evaporated by interaction with the environment. Following Springel et al. (2001), we call structures that can be identified only at one output redshift *volatile*, and do not consider them further.

All star particles that never belong to any galaxies identified in the selected redshift outputs are also assigned to this volatile class. Such star particles either do not belong to any bound structure already at the first output redshift, at $z = 3.5$, or they form in a galaxy *and* become unbound between two simulation output redshifts. In both cases, since we cannot assign those stars to the history of any galaxies, we cannot determine their dynamical origin.

An important issue in our study concerns the reliability of the simulated galaxy population. If galaxies are under-dense, they can easily lose stars or be completely disrupted as a consequence of numerical effects. In simulations, low-mass galaxies may have typical sizes of the order of the adopted softening parameter, so that their internal mass density is underestimated. Therefore at the low-mass end, we expect that our simulated galaxies will have an internal density which is an *increasing* function of galaxy mass. On the other hand, numerical effects should be less important for the more massive galaxies.

To investigate this issue, we evaluate the stellar density of all the simulated galaxies at the half-mass-radius, and plot these in Figure 1 as a function of the galaxy mass, combining all redshift outputs. For real galaxies, the internal density of (early–type) galaxies is a decreasing function of their mass, as shown most recently by Shen et al. (2003), who measured the size distribution for 140,000 galaxies from the Sloan Digital Sky Survey. We use their measured size distribution to estimate the observed galaxy densities within the half-mass-radius. For this purpose, we take the expressions for a Hernquist profile in (Hernquist 1990) to relate Sersic half-light radii to three-dimensional half-mass radii, and then convert the Sersic size-stellar mass relation for early-type galaxies of Shen et al. (2003) to a relation between stellar mass and mean density within the half-mass radius. The solid line in Fig. 1 represents the resulting estimate of the mean galaxy density, with the dotted lines limiting the 3σ scatter of the size distribution as reported in Shen et al. (2003). The dots in Fig. 1 show the equivalent mean densities of our simulated cluster galaxies. In what follows, we use the lower 3σ envelope to estimate the minimum acceptable galaxy densities

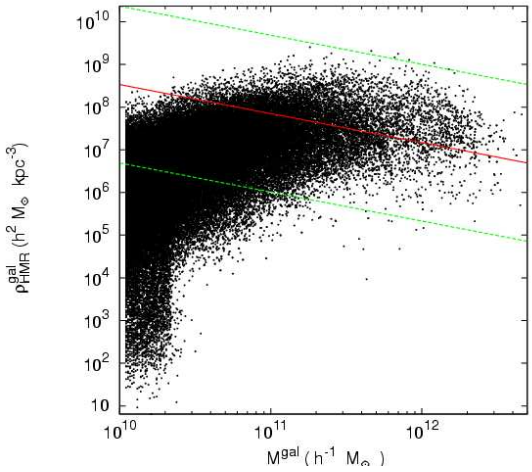

Figure 1. The mean galaxy stellar density inside the half-mass-radius as a function of galaxy mass. All galaxies identified in the parent simulation at all 17 redshift outputs are shown. The solid line shows an estimate of the observed galaxy densities from SDSS data (see text). The dotted lines show the densities corresponding to the 3σ scatter reported in Shen et al. (2003).

$\rho_{\rm min}(M_{\rm gal})$. Galaxies with density lower than this minimum density are discarded and also classified as volatile. From Fig. 1 we note that the observed trend of decreasing density with increasing mass is recovered in our (lower-resolution) parent simulation for galaxy masses $\gtrsim 10^{11} h^{-1} M_\odot$.

In order to quantify the effect of volatile galaxies on our final results, we tested other density thresholds, namely (i) one corresponding to 1σ scatter in the R_e distribution, (ii) a fixed value of $\rho = 5 \cdot 10^6 h^2 M_\odot$/kpc^3, as well as (iii) a galaxy mass threshold, $M = 6 \cdot 10^{10} h^{-1} M_\odot$. Our results remain qualitatively unchanged when either of these criteria is adopted.

4 IDENTIFYING THE DIFFUSE STELLAR COMPONENT

The star formation model implemented in our simulations is based on a gas–density threshold criterion (Springel & Hernquist 2003). This ensures that stars can only form inside existing gravitational potential wells, so that star formation does not take place outside DM halos. Thus DSC stars must have become unbound from their parent galaxies sometime after their formation. Therefore in our analysis, we define as diffuse stellar component (DSC) all those star particles which (i) do not belong to any self-bound galaxy at $z = 0$, (ii) were part of a non-volatile structure at earlier redshifts whose density exceeded the minimum density for its mass as defined above.

In surface brightness measurements of the DSC, sometimes a distinction is attempted between the component associated with the halo of the central dominant (cD) galaxy and the intra–cluster light, which fills the whole cluster region. Quoting from Uson et al. (1991): *"whether this diffuse light is called cD envelope or diffuse intergalactic light is a matter of semantics: it is a diffuse component distributed with elliptical symmetry at the canter of the cluster potential*". In our analysis, we will not make such a distinction: all star particles that do not belong to any self-bound galaxy at $z = 0$, including the cD galaxy identified by SKID, are part of the diffuse

[1] See `http://www-hpcc.astro.washington.edu/tools/skid.html`

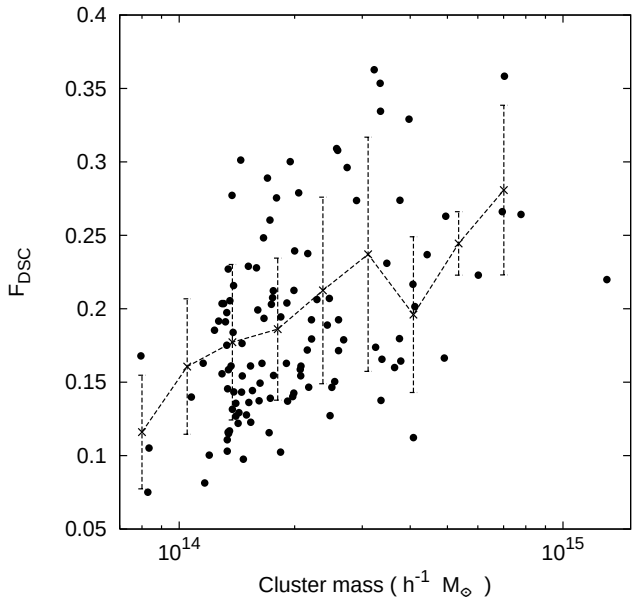

Figure 2. The fraction of stellar mass in the DSC relative to the total stellar mass as a function of the cluster virial mass. Dots are for the 117 clusters in our parent simulation. The crosses show the average values of this ratio in different mass bins, with the error bars indicating the r.m.s. scatter within each bin.

stellar component if they were once part of a non-volatile, above minimum-density structure.

The part of the DSC contributed by galaxies which have a central density lower than $\rho_{\rm min}$ is not considered in our analysis, because it is most likely affected by numerical effects. These low-density structures include a population of extremely low–density objects found by SKID at the very low mass end, many of them representing a mis–identification of SKID due to their small number of particles (< 100). However, by discarding the contribution from low-density and volatile galaxies, we may also neglect a possibly genuine contribution to the DSC from a population of low–mass galaxies. Because of this, our estimate of the diffuse light fraction in the simulated clusters may be an underestimate, although we believe the corresponding bias to be relatively small; we shall discuss this issue in Sect. 6.

Figure 2 shows the fraction $F_{\rm DSC} = M^*_{\rm DSC}/M^*_{\rm tot}$, where $M^*_{\rm DSC}$ is the stellar mass in the DSC and $M^*_{\rm tot}$ is the total stellar mass found within $R_{\rm vir}$ for each cluster in the parent simulation, as a function of the cluster mass. In this computation, the diffuse star particles from volatile galaxies have been discarded. We report on the fractions of DSC stars in all the steps of our selection procedure in Table 1.

Consistent with the results shown in M04, we find: 1) The fraction of DSC relative to the total stellar light in clusters increases with cluster mass, albeit with a large scatter, and 2) the DSC fraction in the simulated clusters is in the range $0.1 < F^{obs}_{\rm DSC} < 0.4$. Both results are broadly consistent with the observed trends and values (Arnaboldi 2004; Aguerri et al. 2005, 2006); however, a direct comparison between observed and measured values of $F_{\rm DSC}$ is only qualitative, because simulations provide the volume–averaged mass fraction directly, while this is not true with the observed DSC fractions.

5 TRACING THE ORIGIN OF THE DSC

The large set of simulated clusters extracted from the cosmological simulation allows us to perform a statistical study of the origin of the DSC. From Fig. 2, it is clear that clusters with similar mass can have rather different amounts of DSC at $z = 0$. For this reason, we will first address the general trends in the origin of the DSC that are independent of the characteristics and dynamical history of individual clusters, such as the redshift at which the most of the DSC becomes unbound, and from which galaxies the intracluster stars mainly originate. We will then investigate whether significant differences in the production of the DSC can be found between clusters belonging to different mass classes, and discuss the robustness of our results against numerical resolution.

We study the origin of the DSC by adopting the following strategy: we follow back in time all the particles in the DSC component at $z = 0$ within each cluster's virial radius and associate them with bound structures present at any earlier redshifts. For all clusters and the 17 redshift outputs (from $z = 0$ to $z = 3.5$), we compile the list of all galaxies as described in Sect. 3. Subsequently, for each DSC particle at $z = 0$, we check whether it belong to any of these galaxies at earlier redshift. If no galaxy is found, the DSC particle is discarded, because we cannot establish its origin. If a galaxy is found, then there are three options:

- This galaxy has a central density larger than the adopted threshold and it belongs to the "family tree" of a galaxy identified at $z = 0$ (see the next subsection); the DSC particle is then associated with that family tree.
- This galaxy has a central density larger than the adopted threshold, but it does not belong to a family tree of any galaxy at $z = 0$; the DSC particle is then considered to come from a "dissolved" galaxy.
- This galaxy has a central density below the adopted threshold and is thus considered as "volatile"; the DSC particle is then discarded.

In this way, the progenitors of all retained DSC particles can be found.

5.1 Building the family trees of galaxies

We build the merger trees of all galaxies identified at $z = 0$, and refer to them as "family trees" to distinguish them from the standard DM halo merger trees.

The "family trees" are built as follows. For each output redshift z_{i+1} of the simulations, we follow all the DM, star and gas particles within the virial radius of the identified cluster at $z = 0$. We build catalogs of all galaxies from the corresponding star and DM particles distributions. For a given galaxy identified at redshift z_{i+1}, we tag all its star particles and track them back to the previous output redshift z_i. We then make a list of the subset of all identified galaxies at z_i which contain the tagged particles belonging to the specified galaxy at z_{i+1}.

We define a galaxy G_i, at output redshift z_i, to be progenitor of a galaxy G_j at the next output redshift z_{i+1} if it contains at least a fraction g of all the stars ending up in G_j. The definition of progenitor depends on the fraction g. Our tests show that the number of galaxies identified as progenitors is stable for g values varying in the range 0.3–0.7. The value adopted for our analysis is $g = 0.5$, which is the same value adopted in several reconstructions of the DM halo merger trees presented in the literature (Kauffmann 2001; Springel et al. 2001; Wechsler et al. 2002).

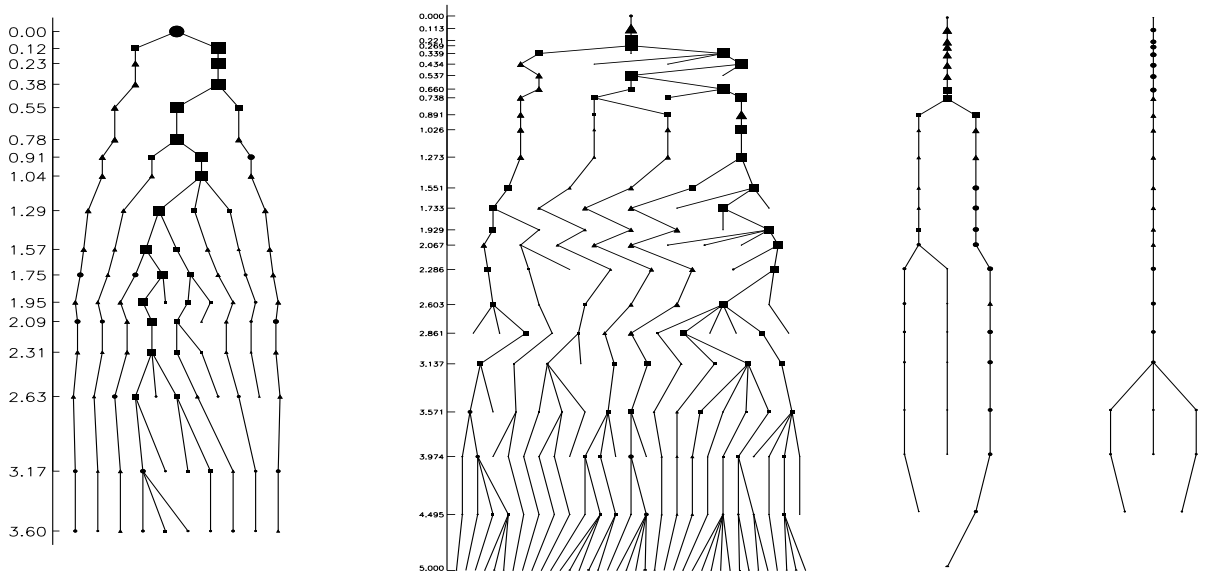

Figure 3. Left: Family tree of the cD galaxy of cluster A in the low-resolution simulation (see Table 1). Right: Family trees of the cD galaxy, the third-most massive galaxy, and a lower-mass galaxy in the high-resolution re-simulation of the same cluster. – The size of symbols is proportional to the logarithm of the mass of the galaxies at the corresponding redshift. Shown on the vertical axis on the left are the output redshifts used to reconstruct the family trees; these are different in both simulations. A galaxy in these trees is considered a progenitor of another galaxy if at least 50% of its stars are bound to its daughter galaxy, according to the SKID algorithm. Many more galaxies can be identified in the high-resolution simulation at similar redshift. The cD family tree is characterised by one dominant branch with a number of other branches merging into it, at both resolutions. Squares and triangles represent our classification of "merging" and "stripping" events, see Section 5.6. Circles correspond to redshift at which the galaxy is not releasing stars to the DSC.

We then build the family trees for all galaxies found at $z = 0$ in all the 117 clusters of our sample. Given the adopted mass threshold of 32 star particle per galaxy, this amounts to an overall number of 1816 galaxies at redshift $z = 0$, and 71648 galaxies in all redshift outputs.

Figure 3 shows the family tree of the cD galaxy of a cluster having virial mass $M\mathrm{vir} = 1.6 \times 10^{14} h^{-1} M_{\odot}$ (cluster A in Table 1). The cD galaxy family tree is complex and resembles a typical DM halo merger tree, with the cD being the result of a number of mergers between pre–existing galaxies. Other galaxies have a much simpler formation history, with fewer or no mergers of luminous objects. This is illustrated in the right part of Fig. 3 which shows merger trees from the high-resolution re-simulation of the same cluster, for the cD galaxy, the third-most massive galaxy in the cluster, and a low-mass galaxy. In more massive clusters, galaxies whose family trees are intermediate between that of the cD and the third-most massive galaxy can also be found. They are however among the most massive galaxies in their cluster, and they are often the most massive galaxy of an infalling subcluster, which has not merged completely with the main cluster yet.

Once the family trees of all galaxies in our clusters at $z = 0$ are built, we then analyse the formation history of the DSC.

5.2 The epoch of formation of the DSC

As already discussed, the star formation model used in our simulations implies that stars can only form inside existing gravitational potential wells, so that all DSC stars must have become unbound from their parent galaxies sometime after their formation. In Figure 4, we plot the fraction of star particles in the DSC at $z = 0$ which are already in the DSC at redshift z. The bulk of the DSC is created after $z \approx 1$, when on average only ≈ 30 per cent of $z = 0$ DSC star particles already reside outside their parent galaxies, with significant cluster-to-cluster variations. However, from the inset of Fig. 4 we note that the production of the DSC follows a power-law, thus implying that it is a cumulative process which, on average, does not have a preferred time scale. Willman et al. (2004) found a similar result based on the analysis of their high–resolution sim-

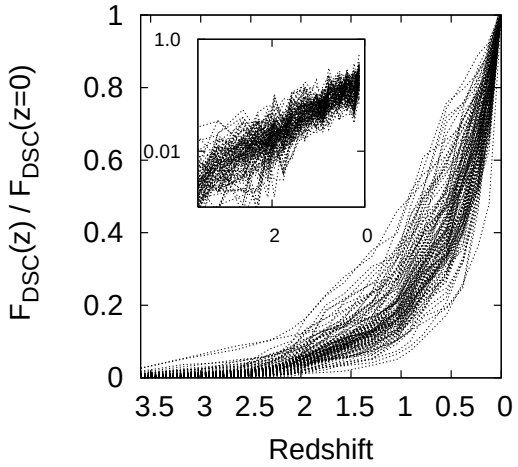

Figure 4. Fraction of star particles found in the DSC at redshift $z = 0$ which are already in the diffuse component at redshift z, for all clusters in our set. The inset show the same curves in logarithmic coordinates.

ulation of a single cluster, with a continuous growth of the DSC fraction and no preferred epoch of formation.

No statistically significant correlation is found between the fraction of DSC at $z = 0$ and a number of possible tracers of the dynamical history of the cluster, such as the concentration of the NFW profile, the number of (DM–halo) major mergers, or the epoch of the last major merger. This suggests that the process of formation of the DSC is more related to the local dynamics of the interactions between galaxies and the group/cluster environment, rather than to the global dynamical history of the cluster.

5.3 DSC and the history of galaxies

We now proceed to establish which galaxies are the main contributors to the formation of the DSC. For each DSC star particle at $z = 0$, we look for a G_j galaxy at z_i to which it last belonged. When this galaxy is found, we check whether the galaxy G_j is associated with the family tree of a galaxy G_k at $z = 0$. If so, then the DSC star particle is associated with the "family tree" of the galaxy G_k. If the G_j galaxy at z_j is not associated with the family tree of any G_k galaxies at $z = 0$, but its family tree ends at z_{j+m}, then the DSC star particle is associated with a dissolved galaxy. If no bound structure is found, then the particle is associated with a *volatile* structure, and it is not considered in the subsequent analysis.

As a next step, we compute what fraction of the DSC particles comes from the family trees of galaxies at $z = 0$, as a function of the binned galaxy mass at $z = 0$, $M_{\rm gal}(z = 0)$. Then the DSC mass $M^*_{\rm DSC}(M_{\rm gal})$ obtained for each $M_{\rm gal}(z = 0)$ bin is normalised by the total stellar mass of the respective cluster. The total fraction $F_{\rm DSC}$ for each cluster is finally given by the sum over all contributions from all galaxy masses at $z = 0$.

5.4 Standard resolution simulation - 4 exemplary clusters

We discuss the results of this analysis for the four clusters shown in Figure 5. The figure shows the density distribution of DM and star particles in the four clusters, and also the distribution of star particles in the high-resolution re-simulation of these clusters. The main characteristics of these clusters are given in Table 1. The galaxies identified by SKID correspond to the densest regions plotted in yellow in this Figure.

These four clusters cover a wide range of masses (see Table 1), and the two intermediate mass clusters B and C have very different dynamical histories: cluster B experienced a major merger at $z \approx 1$, while cluster C is undergoing a merger event at $z = 0$ which began at $z \approx 0.2$.

In Figure 6, the histograms show the mass fractions of the DSC associated with the family trees of $M_{\rm gal}(z = 0)$ galaxy for these four clusters. From Fig. 6, we can draw the following picture for the origin of the DSC:

- The bulk of the DSC comes from the formation history of the most massive galaxy, except in the most massive cluster D;
- Dissolved galaxies give a significant contribution in two out of the four clusters (clusters B,D);
- All other galaxy family trees provide either a small (clusters A–C) or modest (cluster D) contribution to the DSC.

In the case of the most massive D cluster, a significant contribution to the DSC comes from intermediate–mass galaxies. Willman et al. (2004) also found in their simulation of one cluster with mass similar to our cluster D, that galaxies of all masses contributed to the production of the DSC. Our results suggest that when the cluster statistics is enlarged, such cases are rare; in our set this is the case in 3 clusters out of the 11 most massive ones from the whole set of 117 clusters.

Furthermore, Figure 5 shows that cluster D is still dynamically young, with a number of massive substructures both in the DM and in the star particle distribution. This is probably the main reason why the DSC formation in this cluster is not dominated by the most massive galaxy: the sub–clumps contain galaxies of various masses which experienced several mergers in their history, producing a significant amount of DSC. This is also confirmed by the analysis of the family trees of the galaxies belonging to this cluster: 12 of the 85 identified galaxies had more than one merger in their history, while usually only one or two galaxies in each cluster are found to have a complex family tree.

In the other 3 clusters, the largest fraction of the DSC star particles is associated with the formation history of the cluster's most massive galaxy. Cluster B also shows a large contribution coming from dissolved galaxies: perhaps this suggests that the tidal field associated in this cluster was more efficient in disrupting galaxies rather than stripping some of their stars.

Our analysis so far does not exclude that some fraction of the DSC at $z = 0$ is produced in subclusters or groups, such as suggested by Rudick et al. (2006). In fact, the analysis of cluster D suggests that this does happen. If these sub-clusters or groups migrate to the centre of the cluster and finally merge, our procedure would associate the DSC particles unbound from these structures with the family tree of the cD at $z = 0$.

However, if tidal stripping of the least–bound stars in all galaxies were the main mechanism for the production of the DSC, we would expect a more similar fraction of DSC star particles from all galaxy masses.

5.5 Standard resolution simulation - statistics for 117 clusters

We now turn to the statistical results for the whole set of 117 clusters. In Figure 7 we show the contributions from the same galaxy mass bins as before, but averaged over all clusters and over different cluster mass ranges. To obtain our average values, we sum the mass of diffuse star particles in all clusters in the appropriate galaxy mass bin and normalise it to the total stellar mass of all clusters. This procedure creates a "stacked-averaged" cluster. The average value of the diffuse light fraction is $< F_{\rm DSC} >= 16\%$ of the total stellar mass.

In the upper left panel of Fig. 7, showing the fractional contributions from galaxy mass bins averaged over the whole cluster set, the rightmost column represents the contribution from the clusters' BCGs only. The value of the mass for this class is arbitrary; this bin has been plotted separately since the masses of the BCGs increase with cluster mass and, therefore, BCGs in different clusters can belong to different mass bins. This effect is clearly visible in the upper right panel of Fig. 7, which refers to the less massive clusters in our set. For these clusters, the BCGs fall into two mass bins, with the majority of them falling in the second most massive bin.

The other three panels of Fig. 7 show the same relative contributions when the average is performed over (i) the 11 most massive clusters (lower right panel, $M_{\rm vir} > 4 \times 10^{14} h^{-1} M_\odot$ with $< F_{\rm DSC} >= 19\%$), (ii) the 35 clusters having intermediate mass (lower left panel, $2 \times 10^{14} < M_{\rm vir} < 10^{14} h^{-1} M_\odot$ with $< F_{\rm DSC} >= 18\%$), and (iii) the 71 least massive clusters (upper right panel, $M_{\rm vir} < 2 \times 10^{14} h^{-1} M_\odot$ with $< F_{\rm DSC} >= 13\%$).

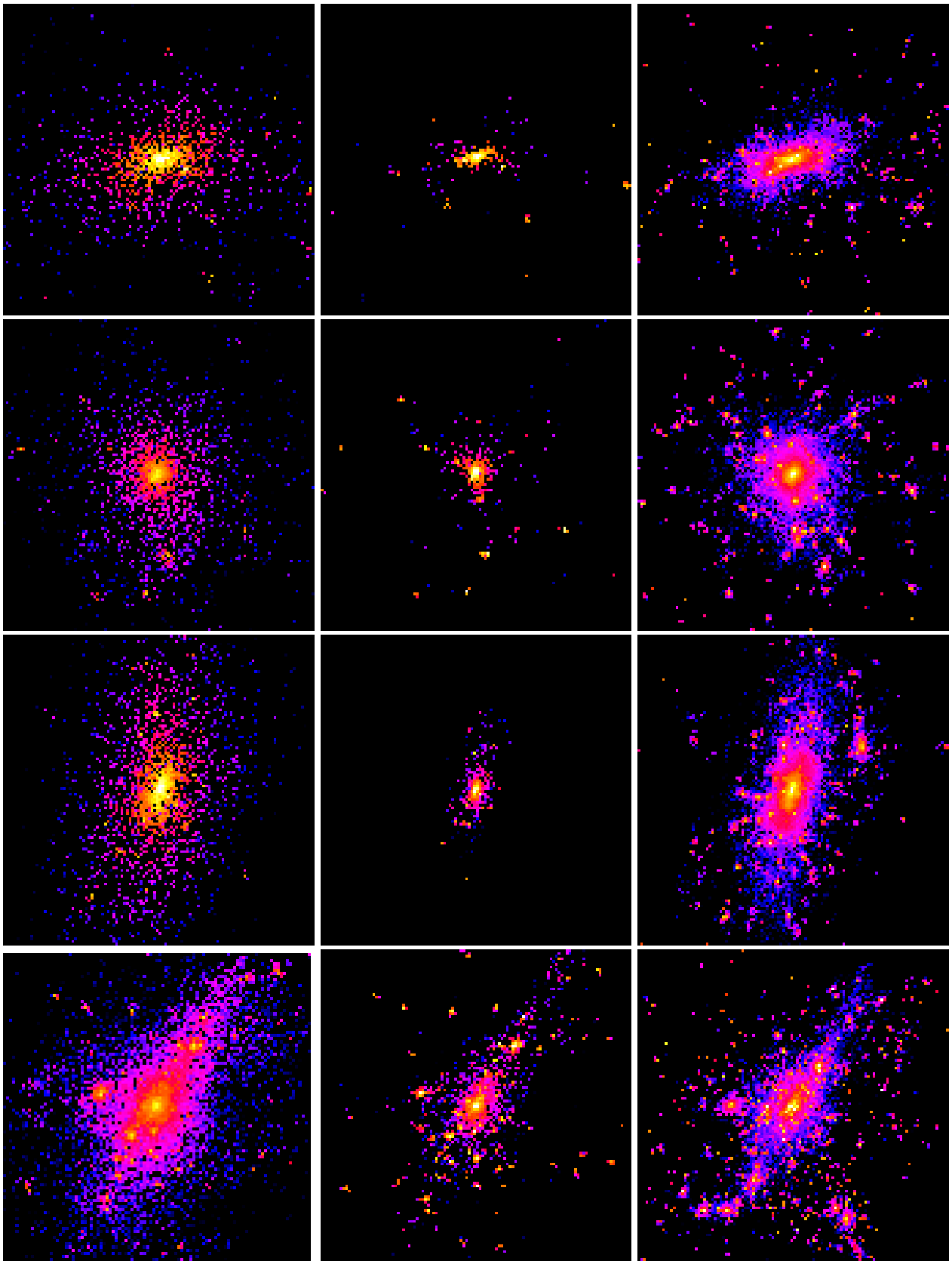

Figure 5. The distribution of the dark matter (left panels) and of the stars (canter panels) for clusters (A), (B), (C), (D) from the cosmological simulation, and the distribution of stars in the high-resolution re-simulations of the same four clusters (right panels), all at redshift $z = 0$. The frames are $3h^{-1}$ Mpc on a side in the first three rows and $6h^{-1}$ Mpc in the last row, corresponding to $\approx 2R_{\rm vir}$ for the four clusters (see Table 1). They show density maps generated with the SMOOTH algorithm, applied separately to the DM and star particle distributions. Colour scale is logarithmic and different for DM and stars: from $10^{-0.5}$ to 10^5 times critical density and from 10 to 10^6 times critical density for stars and DM particles, respectively.

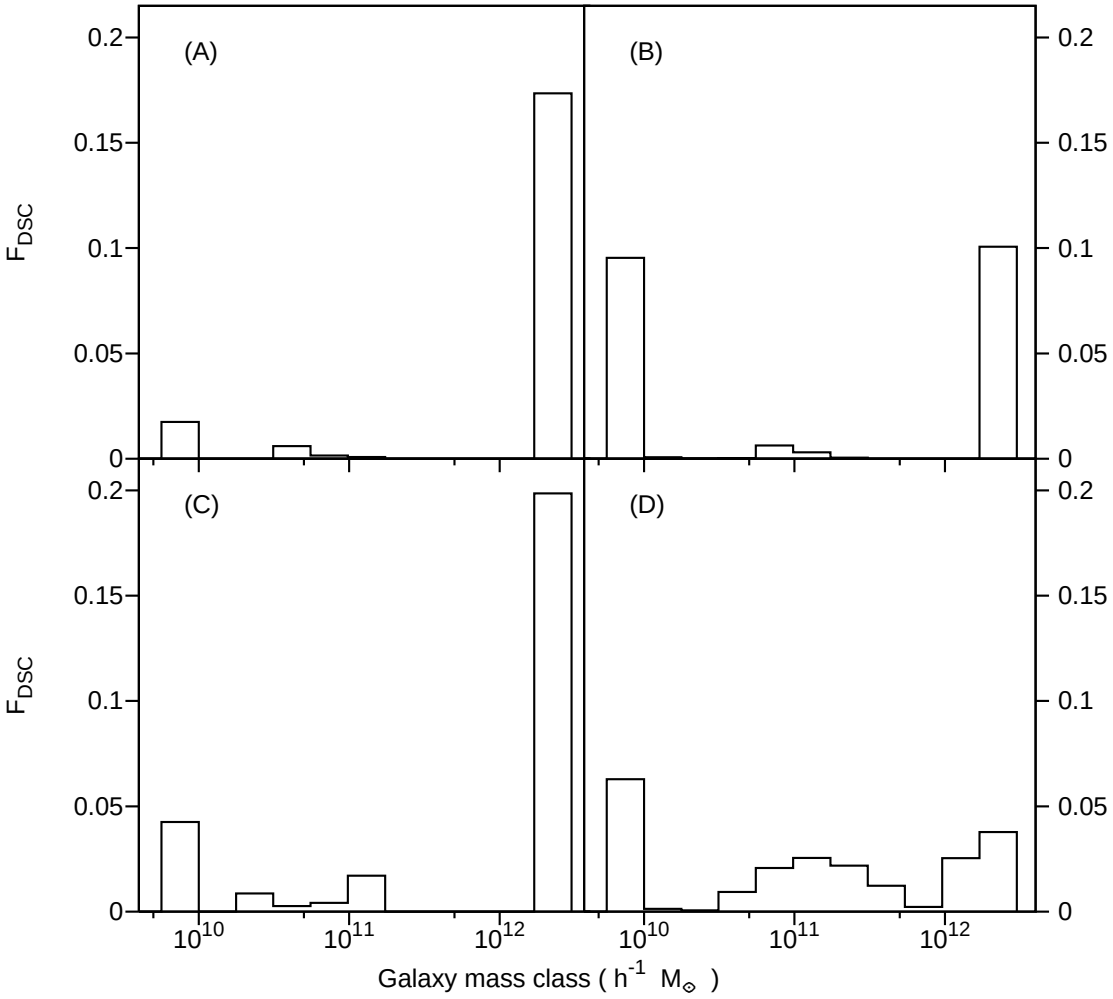

Figure 6. Histograms of the fraction of DSC star particles identified at $z = 0$, associated with the family trees of $z = 0$ galaxies of different masses: $F_{\rm DSC}(M_{\rm gal}) = M^*_{\rm DSC}(M_{\rm gal})/M^*_{\rm tot}$. Results are reported for the four clusters shown in Figure 5 (see also Table 1). We use 10 galaxy mass bins, logarithmically spaced, from $M_{\rm min} = 1.1 \times 10^{10} h^{-1} M_\odot$ to $M_{\rm max} = 3.1 \times 10^{12} h^{-1} M_\odot$. The leftmost column in each panel gives the contribution from dissolved galaxies, regardless of their mass. It is the mass range only for sake of clarity. For these 4 clusters, the only family tree contributing to the rightmost column is that associated with the BCG.

Table 1. Virial masses, viral radii, and DSC fractions for the four clusters A–D shown in Figure 5. The fraction shown in the column 4, $F^{\rm all}_{\rm DSC}$, includes the contribution from low-density galaxies. The $F_{\rm DSC}$ value in column 5 is obtained omitting the particles unbound from low-density galaxies. For completeness we report the fraction $F^{\rm vol}_{\rm DSC}$ of discarded particles from low-density or volatile structures in column 6; the fraction $F^{\rm dis}_{\rm DSC}$ of star particles from dissolved galaxies in column 7, which corresponds to the leftmost columns in the histograms of Figs. 6 and 7; the fraction $F^{\rm ng}_{\rm DSC}$ of star particles that never belonged to any galaxy in column 8. The last row of the table reports the average DSC fractions for the whole sample of 117 clusters.

Label	$M_{\rm vir}$ ($10^{14} h^{-1} M_\odot$)	$R_{\rm vir}$ (h^{-1} kpc)	$F^{\rm all}_{\rm DSC}$	$F_{\rm DSC}$	$F^{\rm vol}_{\rm DSC}$	$F^{\rm dis}_{\rm DSC}$	$F^{\rm ng}_{\rm DSC}$
A	1.6	1200	0.33	0.20	0.11	0.02	0.02
B	2.5	1290	0.36	0.21	0.12	0.10	0.05
C	2.9	1350	0.45	0.27	0.14	0.04	0.04
D	13.0	2250	0.45	0.22	0.23	0.06	0.00
Ave	–	–	0.34	0.18	0.09	0.04	0.07

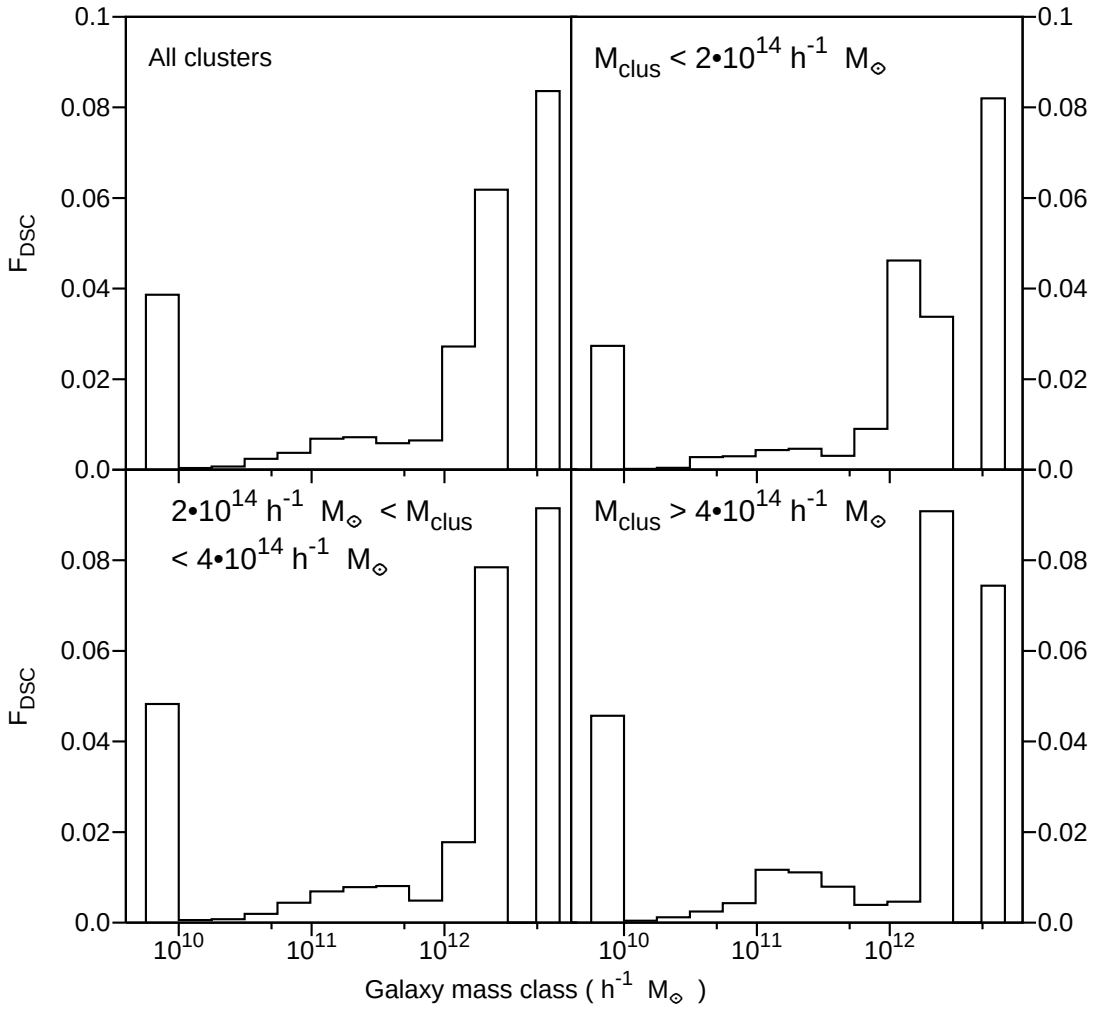

Figure 7. Histograms of the relative contribution to the DSC from the formation history of galaxies belonging to 10 $M_{\rm gal}(z=0)$ mass bins, for the entire set of clusters in the simulation, and as a function of cluster mass. Upper left panel: average over the whole 117 cluster set. Upper right panel: average over the 71 least massive clusters. Lower right panel: average over the 11 most massive clusters. Lower left panel: average over the 35 intermediate–mass clusters. We use 10 $M_{\rm gal}(z=0)$ mass bins, logarithmically spaced from $M_{\rm min}=1.1\times10^{10}h^{-1}M_{\odot}$ to $M_{\rm max}=3.1\times10^{12}h^{-1}M_{\odot}$. The leftmost column in each panel represents the contribution from dissolved galaxies, regardless of their mass. The rightmost column in each panel shows the contribution from the history of the single most massive galaxy of each cluster, regardless of its actual mass.

These average values show a weak trend with cluster mass in the production of the DSC. As a further test, we have divided clusters according the amount of the DSC fraction itself. This analysis also confirms that the dominant contribution to the DSC comes from the BCG family tree, independent of $F_{\rm DSC}$ as expected, given the weak relation between $F_{\rm DSC}$ and cluster mass. We also find that the contribution from dissolved galaxies is slightly higher for clusters with $< F_{\rm DSC} >$ greater than 25%.

The results shown in Fig. 7 are consistent with the previous analysis of the four clusters: the bulk of the DSC is associated with the galaxies in the family tree of the most massive galaxy of each cluster. Galaxies in the family trees of smaller $z=0$ mass bins contribute only few tenths of the fraction from the BCG family tree.

Dissolved galaxies also contribute significantly to the DSC, but it is possible that their estimated contributions are affected by some numerical effects. In fact, if the analysis is restricted to galaxies whose density is within 1σ of the observed galaxy density estimate (Section 3), then the contribution to the $F_{\rm DSC}$ from the BCG rises to $\approx 76\%$, while that from dissolved galaxies drops to $\approx 8\%$. As expected, most "dissolved galaxies" are those with low densities, which indicates that their contribution to the DSC may be affected by the limits in numerical resolution. This needs further work to be properly understood.

5.6 Merging and stripping in galaxy family trees

As shown in Fig. 3, the BCG is the galaxy that experiences the largest number of luminous mergers during its assembly, and it often has the most complex family tree in a cluster. Our result that a large fraction of DSC is associated with the BCG supports a scenario where mergers release stars from their parent galaxies to the intracluster space.

To investigate this further, we estimate the fraction of DSC particles associated with the *merger* part of the family trees, and

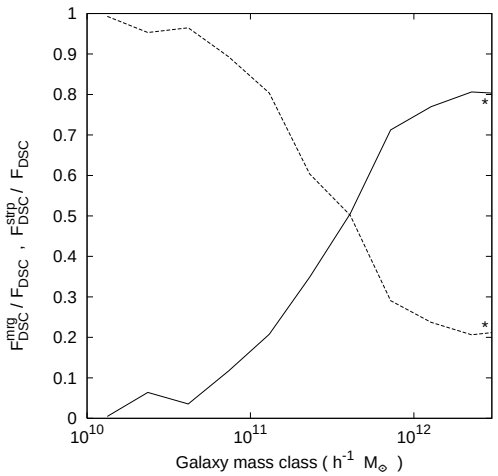

Figure 8. The fraction of DSC stars arising in the "merger" part, $F^{\rm mrg}_{\rm DSC}/F_{\rm DSC}$, and in the "stripping" part, $F^{\rm strp}_{\rm DSC}/F_{\rm DSC}$, of the galaxy family trees, as a function of their $z = 0$ galaxy mass class (solid and dashed lines, respectively). The asterisks mark the values for the contribution from the BCG family tree only. See text for details.

with the *stripping* part of the family trees, as follows. We define a DSC star particle to arise from a *merger* at redshift z_j if the galaxy it was last bound to has more than one progenitor at z_{j-1}[2]. The DSC particles coming from the progenitors at z_{j-1} are also defined as arising from a merger. We take a DSC star particle to be unbound through *stripping* if the galaxy it was last bound to at redshift z_j has only one progenitor at z_{j-1}. The different parts of the family trees are indicated in Fig. 3, where the squares represent the *merger* part of the tree, triangles the *stripping* part, while circles mark the part of the tree where no stars are released to the DSC.

In Figure 8, we show the fraction of the DSC star particles which arise from the *merger* part of the family tree, as a function of the final galaxy mass. For high–mass galaxies, most of the DSC originates from the *merger* part of their family trees. Low mass galaxies, on the other hand, lose stars only via *stripping*. After each *merger* between massive galaxy progenitors, up to 30% of the stellar mass in the galaxies involved has become unbound. This large fraction perhaps indicates that many of these mergers take place either in strong tidal fields generated by the mass distribution on larger scales, or just before the merger remnants fall into their respective cluster.

Combined with the result that most of the DSC star particles are associated with the family trees of the most massive galaxies, the fact that most of the DSC is released during *merger* events implies that the bulk of the DSC originates in the merger assembly of the most massive galaxies in a cluster. The more standard picture for the formation of the DSC, in which all galaxies lose their outer stars while orbiting in a nearly constant cluster gravitational potential, is not confirmed by current cosmological hydrodynamic simulations. It appears that strong gravitational processes, linked to the formation of the most massive galaxies in the cluster and to mergers between luminous objects, are the main cause for the creation of the DSC.

A further mechanism possibly at work is the complete disruption of galaxies, which also takes place preferentially in the cluster central regions. In our cosmological simulation this formation mechanism for the DSC is likely to be enhanced by numerical effects, which tend to produce under-dense galaxies. We address this issue below when we discuss our high-resolution simulations of the clusters in Fig. 5.

5.7 cD Halo *vs* Intracluster Light

So far, we have made no attempt to distinguish between a component of DSC associated with the unbound halos of the central cD galaxies, and a more cluster-wide DSC. Our definition of the DSC includes stars in the cluster central regions and a part of these may well be in the form of cD halos (see the Appendix). Independent of how well a distinction between these two components can be made, one might expect that the fraction of DSC stars that comes from the merging tree of the BCG would be most concentrated towards the cluster centre. To shed some light on this question, we show in Figure 9 the same analysis for the average over all galaxy clusters in the simulation as in Fig. 7, but now excluding all DSC particles residing in the central $250h^{-1}$ kpc around their cluster centres. The remaining total DSC fraction drops to about 6%, less than half of the total, reflecting the steep radial profile of the DSC (Murante et al. 2004; Zibetti et al. 2005). For $R > 250h^{-1}$kpc, the family trees of the most massive galaxies still provide the largest contribution to the DSC (per mass bin), but the cumulative contributions from family trees of less massive galaxies now dominates the BCG component by a factor ~ 2. At the same time, the relative contribution from dissolved galaxies increases. The lower panel of Fig. 9 shows the same analysis but now excluding DSC particles within $0.5R_{\rm vir}$. In this case, the $< F_{\rm DSC} >$ drops to $\sim 1\%$, with the fraction from the BCG family tree now similar to that from other galaxies.

Since the BCG halo is likely to be less extended than $250h^{-1}$ kpc, our interpretation of the results in Fig. 9 is that the *merger* part of the most massive galaxy family tree in each cluster contributes substantially to the DSC also outside the cD halo. However, at radii $250h^{-1}$kpc $< R < 0.5R_{\rm vir}$, the cumulative contribution from the family trees of other massive galaxies dominates the DSC. Presumably, these are the most massive galaxies within subgroups, which fell into the cluster and brought in their own DSC, but which have not yet had time to merge with the BCG. This interpretation is consistent with the simulation results of Willman et al. (2004) and Rudick et al. (2006). Only in the outskirts of clusters, at $R > 0.5R_{\rm vir}$, we find that the DSC particles come preferentially from the *stripping* part of family trees from all galaxy mass bins.

The relevance of *merger* events for the formation of the DSC may explain why diffuse light is more centrally concentrated than galaxies, in both observations (Zibetti et al. 2005; Arnaboldi et al. 2002) and in simulations (M04, Willman et al. 2004, Sommer-Larsen et al. 2005). Stars from accreted satellite galaxies form extended luminous halos around massive galaxies (Abadi et al. 2006), and if these massive galaxies end up concentrated to the cluster centre, their diffuse outer envelopes would preferentially contribute to the DSC in the cluster centre.

Our results on the origin of the DSC are also consistent with the predictions by D'Onghia et al. (2005) that simulated fossil galaxy groups have a larger amount of intra–group stars than

[2] It may happen that the final phase of the merger is not detected by our galaxy identification procedure, because the two merging structures are very close to each other and have small relative velocities. In this case, the SKID algorithm generally merges the two objects into a single one, even if the merger is not yet completed. For this reason, we assign a DSC star particle to the merger part of its parent galaxy family tree even if it becomes unbound two family tree levels after the merger, at z_{j+1} (i.e. from the "offspring of the offspring" of a merger).

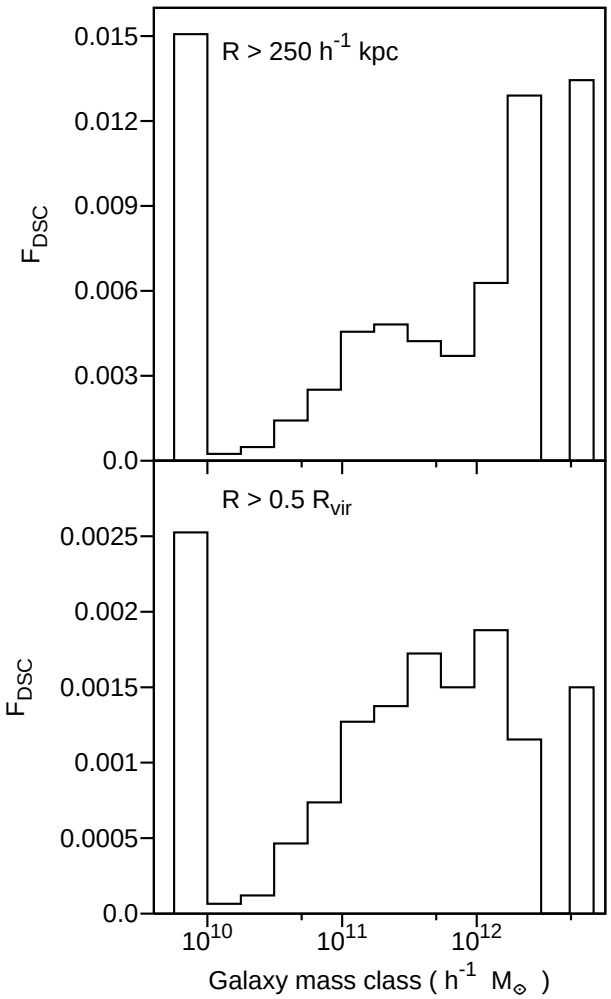

Figure 9. The same as in Figure 7, averaging over all clusters, but excluding the DSC star particles inside $R = 250h^{-1}$ kpc (upper panel) and inside $0.5R_{\rm vir}$ of each cluster (lower panel).

normal groups. Indeed, if fossil groups are the dynamically most evolved groups, then their galaxies had more time to interact and build up the central elliptical galaxy (see e.g D'Onghia et al. 2005). The number of galaxy–galaxy mergers in groups appears to be closely related to the amount of DSC liberated (Sommer-Larsen 2006). A direct comparison of our results with Willman et al. (2004) is difficult because of their re-normalisation of the simulated galaxy luminosities in order to fit the observed luminosity function, but these authors also concluded that luminous galaxies provide a substantial contribution to the DSC.

6 HIGH RESOLUTION SIMULATIONS AND THE EFFECTS OF NUMERICAL RESOLUTION ON THE FORMATION OF THE DSC

To address the stability of our results against mass and force resolution, we have re-simulated three clusters extracted from the cosmological box (A,B,C from Table 1) with 45 times better mass resolution and $\simeq 3.6$ times smaller gravitational softening.[3] A detailed presentation of these re-simulations is given in Borgani et al. (2006). Galaxies formed in these high-resolution simulated clusters have densities similar to those shown in Fig. 1 for masses larger than $\approx 10^{11}h^{-1}M_{\odot}$, and the low–density tail seen in Fig. 1 is shifted towards lower masses, in accordance with the better resolution.

We carry out our study of the DSC in these three clusters following the procedure described previously, discarding DSC star particles contributed from under-dense and volatile structures[4]. In Fig. 10, we show the fractions of DSC star particles identified at $z = 0$ and originating from the history of galaxies belonging to different mass bins. The full columns refer to the analysis of the high–resolution simulations of the three clusters, while the open columns show the results from Fig. 6 for the low-resolution simulations.

In the clusters simulated with high resolution, the results on the origin of the DSC are consistent with what we found for the standard resolution. The DSC builds up in parallel with the formation of the most massive galaxies in the cluster. The amount of DSC star particles produced during the history of all other galaxies is still negligible when compared with the contribution from the most massive cluster members. With the increase in resolution, more DSC stars now come from dissolved galaxies in clusters A and C, and an increasing number comes from the family tree of the cD in clusters A and B.

Another question is whether the results on the DSC are affected by the efficiency of the kinetic feedback from SNe. To address this point, we re-simulate cluster A at the resolution of the cosmological box, with (i) the same feedback efficiency and (ii) the speed of the galactic ejecta set to zero. We find very similar results in the strong and weak feedback cases: no significant contribution from intermediate mass galaxies, 7.5% and 8.7% of the DSC coming from dissolved galaxies, and 89.7% and 87.1% of the DSC originating from the history of the BCG, respectively.

However, the overall fraction of intracluster stars in these three clusters changes between our low-resolution and high-resolution simulations. Once the star particles from volatile and under-dense galaxies are discarded, the fraction of DSC within the virial radius of clusters A, B and C is $F_{\rm DSC} = 0.37, 0.28, 0.41$ in the high resolution simulations, compared with $F_{\rm DSC} = 0.20, 0.21, 0.27$ in the standard resolution case. The overall increase of the DSC fraction at high-resolution is mostly, but not only, related to an increase in the fraction of DSC from dissolved lower-mass galaxies (see Fig. 10).

This result is not in contradiction with Sommer-Larsen (2006) finding that the DSC fraction in his simulations remains constant when the resolution is increased. This is because in the Sommer-Larsen (2006) simulations the numerical resolution is increased without adding the corresponding higher frequencies in the initial power spectrum. Then the number of low-mass galaxies and (small–object) mergers does not increase significantly, and one expects an approximately constant DSC fraction. This suggests that the increase in the DSC fraction in our high-resolution simulations is related to the addition of small objects through the added high-frequency part of the power spectrum.

[3] Cluster D has been re-simulated at only 10 times better mass resolution and its analysis is not discussed here.

[4] For the high–resolution clusters we use 24 different redshifts, starting from $z = 5$.

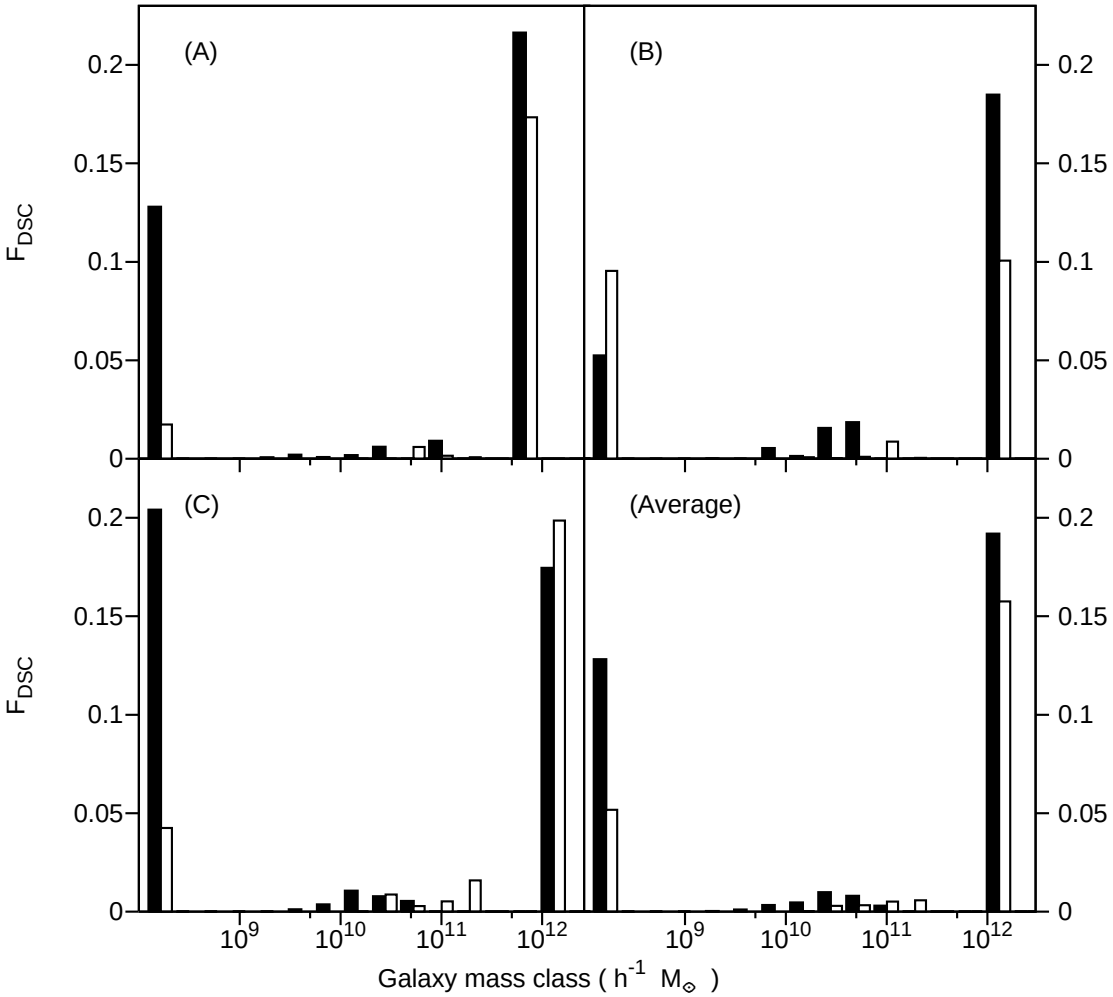

Figure 10. Histograms of the fraction of the $z = 0$ DSC particles associated with galaxy family trees in 15 $M_{\rm gal}, (z = 0)$ mass bins, for the three clusters re–simulated at high–resolution (filled columns), and in the standard–resolution (empty columns, cf. Fig. 6). The mass bins are logarithmically spaced, from $M_{\rm min} = 2 \times 10^8 h^{-1} M_\odot$ to $M_{\rm max} = 3.1 \times 10^{12} h^{-1} M_\odot$. The leftmost columns show the contribution from dissolved galaxies, regardless of their mass. Upper-left, upper-right and lower-left panels show the comparison for clusters (A), (B), (C), respectively; the lower-right panel show the average for these three clusters.

We expect that the effect of numerical overmerging is reduced at higher resolution (e.g., Borgani et al. 2006, and references therein for a full discussion of this issue), so we must look for other effects that could dominate the disruption of the smaller galaxies. The results from Sommer-Larsen (2006) also rule out a significant effect from stronger tidal shocks during high-speed collisions with low-impact parameters, when galaxies become denser at higher numerical resolution. One possibility is that, when the resolution is increased, the number of numerically resolved mergers increases. On the basis of the results reported above, this could turn into an increased efficiency in the production of the DSC. If so, a solution to the problem could lie in a more realistic feedback mechanism.

Another issue related to the numerical resolution concerns the number of small ($\lesssim 10^{11} h^{-1} M_\odot$) galaxies identified in these simulations. Recent determinations of the K–band luminosity function for galaxies in clusters give a faint–end slope between $\alpha = -0.84$ and $\alpha = -1.1$ (Lin et al. 2004). The faint end slope of the stellar mass function in our cosmological simulation is flatter than the observed luminosity function: we obtain $\alpha \approx -0.7$, thus implying that we miss a number of small galaxies. A shallower slope of the faint end of the luminosity function is a general problem of numerical simulations like those presented here (e.g. Willman et al. 2004).

If the number of low–mass galaxies is underestimated in the simulations, then their contribution to the DSC would be affected in the same way. To estimate this effect, we computed how many galaxies we would expect in each mass bin of Fig. 7, if the faint end of the stellar mass function was given by $n(M) = K \cdot (M/M_*)^\alpha$, with $\alpha = -0.84, -1.1$ and $M_* = 5 \cdot 10^{11} h^{-1} M_\odot$. The constant is fixed by requiring that the number of galaxies for a mass $M = 2 \cdot 10^{11} h^{-1} M_\odot$ is the same as in the simulation. This method is similar to the re-normalisation of the luminosity function in Willman et al. (2004). We then assume that the missed galaxies contribute the same relative fraction of their mass to the DSC as the present-day galaxies of similar mass in the simulation, and multiply the fraction $F_{\rm DSC}(M)$ by the ratio of $N(M)/N_s(M)$, where

$N_s(M)$ is the number of simulated galaxies found in the bin and $N(M)$ is the integral of $n(M)$ in the same bin. This correction is applied to each mass bin up to $2 \cdot 10^{11} h^{-1} M_\odot$. Fig. 11 shows the result of this correction when it is applied to the average distribution of $F_{\rm DSC}$ for the whole set of three clusters (lower right panel of Fig. 10). The DSC production is still dominated by the contribution coming from the BCGs in the clusters. The effect of such correction is to bring the contribution of the mass bins corresponding to masses $M < 10^{11} h^{-1} M_\odot$ to the same levels of the others. Correction is stronger for the smaller mass bins. Nevertheless, the contribution of these mass classes to the global $F_{\rm DSC}$ remain small. Note that the increases in $F_{\rm DSC}(M)$ values in the mass bin $\sim 2 \cdot 10^{11} h^{-1} M_\odot$ is due to a few galaxies with mass $1.5 < M < 2 \cdot 10^{11} h^{-1} M_\odot$, whose contribution to the DSC has been corrected. The contribution $F_{\rm DSC}(M)$ from galaxy having masses smaller than $\approx 1.1 \cdot 10^{10} h^{-1} M_\odot$ in the three re-simulated clusters, where they are resolved, is very small.

A further issue to be considered is that all galaxies are spheroidal at the numerical resolution of these cosmological simulations; indeed, the self–consistent formation of disk galaxies is still a challenge in hydrodynamic ΛCDM simulations. Are our conclusions on the origin of the DSC likely to be affected by the absence of disk galaxies in our cosmological simulation? Generally, disk galaxies are more vulnerable to tidal forces, but the amount of matter lost in tidal tails is small, unless the tidal field is very strong, whereas elliptical galaxies lose their outer stars more easily. We do not expect that it would make a lot of difference for the amount of DSC released in the merging processes leading to the formation of the cluster BCG galaxies and most of the DSC, if a fraction of the participating galaxies were disk galaxies. However, this needs to be checked once simulations can reproduce disk galaxies. Independent arguments based on tidal stripping from disk galaxies in a semi–analytical model of galaxy formation (Monaco et al. 2006,?) suggest that at most ~ 10 per cent of the total stellar mass of each cluster is contributed to the DSC by the " quiet tidal stripping" mechanism, even for the most massive clusters where observations points toward a larger amount of diffuse stars.

As already discussed in Section 3, our force resolution is not enough to resolve the inner structure of the simulated galaxies. As a consequence, their internal density is likely to be underestimated, so that these galaxies are more vulnerable to tidal stripping and disruption than real galaxies. This numerical artifact is not completely removed even in our high resolution re-simulations, where the Plummer–equivalent softening is $\simeq 2h^{-1}$ kpc. Even when simulated galaxies with central densities lower than a chosen threshold are removed, we still find that less massive galaxies are less dense than massive galaxies, at variance with observational results. This probably accounts for most of the contribution to the DSC from dissolved galaxies. If we had more realistic, denser small galaxies in the simulation, this might decrease their contribution to the DSC even more.

We can summarise the discussion of systematics effects in our analysis related to numerical resolution as follows:

(i) Our conclusion, that the formation of the DSC is intimately connected with the build–up of the cluster's BCG, is confirmed in higher numerical resolution simulations;

(ii) this conclusion appears insensitive to the limitations of current simulations in reproducing low-mass galaxies, disk galaxies, and the faint-end luminosity function;

(iii) resolving galaxies with smaller masses in the high-resolution simulations does not have a strong effect on the formation and evolution of the DSC;

(iv) the global value of $F_{\rm DSC}$ depends on resolution, and it increases in simulated clusters with higher resolution. The value of this fraction has not converged yet, in the range of numerical resolution we examined.

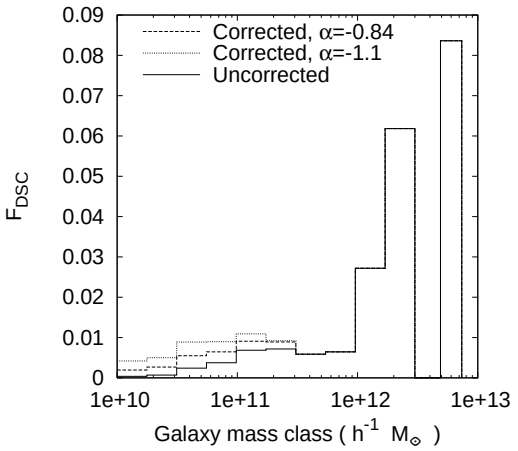

Figure 11. Corrections to $F_{\rm DSC}$ to account for the low–mass end of the galaxy mass function. The solid line is the uncorrected $F_{\rm DSC}$; the dashed and the dotted lines give the corrected value when the low–mass end of the galaxy cluster stellar mass function has a slope $\alpha = -0.84$ and $\alpha = -1.1$, respectively.

7 HOW DO STARS BECOME UNBOUND? ON THE ORIGIN OF THE DIFFUSE STELLAR COMPONENT

In cosmological hydrodynamic simulations, stars form in galaxies. The DSC is built up from stars that are dissolved from their parent galaxies. This is an ongoing process linked to the accretion of substructure (see above and also Willman et al. 2004); in fact, most of the DSC originates at relatively recent redshifts. Stars may be added to the DSC through a number of dynamical processes, listed here in the approximate time sequence expected during the infall of a significant subcluster:

(i) Tidal stripping of the preexisting diffuse stellar population from the in-falling subcluster or group: The DSC in the substructure, generated by dynamical processes in the substructure, is added to the DSC of the main cluster when both structures merge.

(ii) Stripping from extended galaxy halos created in substructures: In subclusters or galaxy groups, galaxy interactions occur with lower relative velocities and are thus generally more damaging than in interactions with the high relative velocities typical for galaxy clusters. Interactions or mergers within substructures may create loosely bound stellar halos which are stripped from their parent galaxies and the substructure when entering the cluster tidal field (Mihos 2004; Rudick et al. 2006). This stripping may be delayed when the merging in the subcluster happens before its accretion, or immediate when the galaxy interactions occur already deep in the tidal field of the main cluster.

(iii) Tidal shocking and stripping during merger with the cD galaxy: The massive galaxies in the substructure generally interact with the cluster centre and the cD galaxy on near-radial orbits (see Figure 12). In a high-speed encounter of a massive galaxy with the cD, stars from both galaxies may gain sufficient energy to

be (almost) tidally unbound from their parent galaxies. The tidally shocked stars from the intruder are then subsequently unbound by the ambient tidal field or further tidal shocks, remaining at similar orbital energies as their mother galaxy had at the time. Those from the cD galaxy become part of the cD envelope. The process may happen several times as the intruder galaxy orbit decays by dynamical friction. This mechanism is related to the cannibalism scenario for the growth of the cD galaxy, described in Ostriker & Hausman (1977); Merritt (1995) and others; however, here the dynamical friction appears to be more effective, presumably due to the large dark matter mass associated with the infalling substructure.

(iv) Tidal dissolution of low-density galaxies: These galaxies may enter high-density regions of the cluster along their orbits, such as the dark matter cluster centre, and dissolve completely if of sufficiently low density.

(v) Tidal stripping in galaxy interactions: Stars may be torn out from galaxies during tidal interactions along their orbits in the cluster, and be dissolved from their parent galaxies by the cluster tidal field. The participating galaxies survive as such. Galaxies of all masses are affected. The last two processes together are often described as harassment (Moore et al. 1996).

The statistical results of the previous sections allow us to put some constraints on the relative importance of these various processes, and to identify further work needed to clarify the origin of the diffuse stellar population in galaxy clusters. These results can be summarised as follows.

- Most of the DSC is liberated from galaxies in the merger tree of the most massive, central galaxy in the cluster, i.e., simultaneously with the build-up of this galaxy.
- If only the fraction of the DSC outside $250\mathrm{kpc}$ from the cluster centre, i.e., outside the cluster dominant galaxy's halo, is considered, the contribution from the BCG family tree is comparable to that from other massive galaxies. Only outside $\sim 0.5R_{\rm vir}$ do galaxies of all masses contribute to the DSC.
- There is a further, sizable contribution to the DSC in the simulations, from dissolved galaxies. However, the fraction of DSC stars from dissolved galaxies depends directly on the simulations' ability to faithfully represent the lower mass galaxies, and is seen to vary strongly with the resolution of the simulation. This contribution to the DSC is thus currently uncertain; the prediction from the simulations is likely to overestimate the contribution of dissolved galaxies to the ICL in observed clusters.
- About 80% of the DSC that comes from the merger tree of the cD galaxy, is liberated shortly before, during, and shortly after major mergers of massive galaxies. About 20% is lost from these galaxies during quieter periods between mergers.
- In each significant merger, up to 30% of the stellar mass in the galaxies involved becomes unbound.
- Most of the DSC is liberated at redshifts $z = 0 - 1$.

These results imply that the main contribution to the DSC in our simulations comes from either tidal shocking and stripping during mergers with the cD galaxy in the final cluster (mechanism iii), and/or from merging in earlier subunits whose merger remnants later merge with the cD (i, ii). The traditional tidal stripping process (v) appears to contribute only a minor part of the DSC but may be the dominant process for the small fraction of the DSC that ends up at large cluster radii.

Further work is needed to see which of the channels (iii) or (i,ii) is the dominant one, and whether in the latter the contribution of the preexisting DSC in the accreted subclusters (i) dominates over that from extended galaxy halos (ii). The work of Willman et al. (2004) and Rudick et al. (2006) shows that the contribution from infalling groups is important but the division between the channels (i) and (ii) is not clear. In this case, our results imply (a) that merging must have been important in these groups, and (b) that the massive galaxies in the infalling groups that carry most of the final DSC will mostly have merged with the BCG by $z = 0$, so that the tidal shocking and stripping process (iii) will play some role as well. The description of D'Onghia et al. (2005) and Sommer-Larsen (2006) of fossil groups as groups that are older than other groups, in a more advanced evolutionary stage with a dominant elliptical galaxy, and with a larger fraction of DSC, suggests dense, evolved groups as promising candidates for contributing significantly to the cluster DSC. One recent observational result that also fits well into this picture of accreting groups that have already had or are having their own merger events, is the observation of Aguerri et al. (2006) that the DSC fraction in Hickson groups correlates with the elliptical galaxy fraction in these groups.

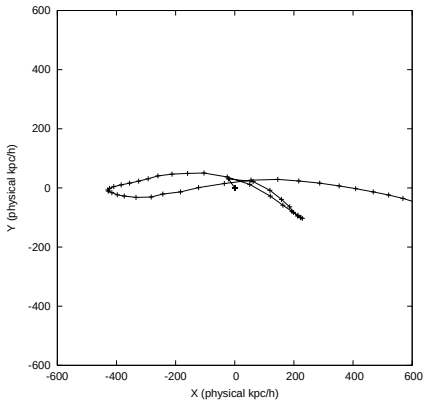

Figure 12. Typical projected orbit of a galaxy ending in a major merger with the cD galaxy; here in cluster A at redshift 0.269.

Certainly it is clear from our results that the formation of the cD galaxy, its envelope, and the DSC in galaxy clusters are closely linked. Further analysis is required to determine whether these components are dynamically distinct, and what kinematic signatures can be used to distinguish between them in observations of cD clusters.

8 CONCLUSIONS

In this paper, we have studied the origin of the diffuse stellar component (DSC) in galaxy clusters extracted from a cosmological hydrodynamical simulation. We identified galaxies in 117 clusters with the SKID algorithm, tracing each of them back in time at 17 different redshifts from $z = 3.5$ to $z = 0$. This allowed us to build the family tree of all galaxies identified at $z = 0$ in all clusters. We find that all BCGs are characterised by complex family trees, which resemble the merging trees of DM halos. At the resolution of our simulation, only a small number of massive galaxies other than the BCGs undergoes several mergers during their past history. The majority of galaxies never have mergers, or only one at very early redshift.

Because of the star formation criteria employed in the simulation, all stars found in the DSC at $z = 0$ were born in galaxies and later dissolved from them. We track each DSC star particle back to the last redshift when it still belonged to a galaxy, and thus

link it to the dynamical history of this galaxy. We exclude all DSC star particles from the analysis which arise from volatile and underdense galaxies; the latter being defined relative to the observational mass–radius relation of early type galaxies by Shen et al. (2003). The main results of our analysis can be summarised as follows.

- The formation of the DSC has no preferred redshift and is a cumulative power–law process up to redshift $z = 0$. We find that $\simeq 70$ per cent of the DSC is formed after redshift $z = 1$.
- We find a weak increase of the final amount of DSC stars with the mass of the cluster, but no significant correlation with the global dynamical history of the clusters.
- For all but the 3 most massive clusters, DSC star particles come mainly from the family tree of the most massive (BCG) galaxy. I.e., the formation of the DSC goes largely in parallel with the build-up of the BCG galaxy.
- Most DSC star particles become unbound during merging phases along the formation history of the BGCs, independent of cluster mass.
- Masking the inner 250 h^{-1} kpc of each cluster, in order to exclude the cD halo from the analysis, does not qualitatively change the emerging picture.

From these results we conclude that the bulk of the DSC star particles are unbound from the galaxy in which they formed by the tidal forces acting before, during, and shortly after merging events during the formation history of the BCGs and other massive cluster galaxies. Only in the outskirts of clusters, $R > 0.5R_{\rm vir}$, we find that galaxies of many different masses provide comparable contributions to the DSC , which is similar to a "quiet stripping" scenario, but the actual mass in DSC stars in these regions is small.

The formation of the BCG in these simulations is related to many mergers which begin early in the history of these galaxies and continue all through $z = 0$. As discussed in the previous section, it is reasonable to infer that the massive elliptical galaxies, which merge with the BCGs, are contributed by infalling groups, which have already generated their own DSC and/or loosely bound halos, as found by Willman et al. (2004) and Rudick et al. (2006). Part of the cluster DSC will also be generated by the tidal shocking and stripping during the merger of these massive galaxies with the BCG itself; the relative importance of these processes is yet to be established.

Since the fraction of diffuse light stars contributed by each accreting group depends on the details of the dynamical history of the group itself, such a mechanism for the generation of the DSC can hide a direct link with the formation history of the clusters. This may be the reason why we do not detect a clear correlation between the $z = 0$ DSC fraction and the cluster formation history.

At the resolution of our (and other similar) simulations, it is not yet possible to resolve the inner structure of low-mass galaxies. We have taken this into account in our analysis by discarding all DSC particles from galaxies with densities below a threshold set by observations. In addition, there are well-known problems in cosmological simulations with forming disk galaxies, and with reproducing the galaxy luminosity function. These issues clearly introduce some uncertainty in the discussion of the origin of the DSC in hydrodynamic ΛCDM simulations. We find that the global amount of DSC in our simulations *increases* with numerical resolution and has not yet converged in the best simulations. Thus a straightforward comparison of observed DSC fractions with numerical simulations is not possible yet. On the other hand, massive galaxies are well-resolved in our simulations, and we believe that our main new result, that a major fraction of the DSC in galaxy clusters is dissolved from massive galaxies in merging events, is a robust one.

ACKNOWLEDGEMENTS

The simulations were carried out at the "Centro Interuniversitario del Nord-Est per il Calcolo Elettronico" (CINECA, Bologna), with CPU time assigned under INAF/CINECA and University-of-Trieste/CINECA grants. This work has been partially supported by the PD-51 INFN grant. OG thanks the Swiss National Science Foundation for support during the early stages of this work under grant 200020-101766. We acknowledge financial support by INAF projects of national interests (PI: M. A.). KD acknowledges support by a Marie Curie fellowship of the European Community program "Human Potential" under contract number MCFI-2001-01221. We acknowledge S. Bonometto, P. Monaco and L. Tornatore for fruitful discussions and V. Springel for kindly providing us the non–public part of the GADGET code.

REFERENCES

Abadi M. G., Navarro J. F., Steinmetz M., 2006, MNRAS, 365, 747
Aguerri J. A. L., Castro-Rodríguez N., Napolitano N., Arnaboldi M., Gerhard O., 2006, A&A, 457, 771
Aguerri J. A. L., Gerhard O. E., Arnaboldi M., Napolitano N. R., Castro-Rodriguez N., Freeman K. C., 2005, AJ, 129, 2585
Arnaboldi M., 2004, in IAU Symposium Intracluster Stellar Population. pp 54–+
Arnaboldi M., Aguerri J. A. L., Napolitano N. R., Gerhard O., Freeman K. C., Feldmeier J., Capaccioli M., Kudritzki R. P., Méndez R. H., 2002, AJ, 123, 760
Arnaboldi M., Freeman K. C., Okamura S., Yasuda N., Gerhard O., Napolitano N. R., Pannella M. E., 2003, AJ, 125, 514
Arnaboldi M., Gerhard O., Aguerri J. A. L., Freeman K. C., Napolitano N. R., Okamura S., Yasuda N., 2004, ApJ, 614, L33
Borgani S., Dolag K., Murante G., Cheng L.-M., Springel V., Diaferio A., Moscardini L., Tormen G., Tornatore L., Tozzi P., 2006, MNRAS, 367, 1641
Borgani S., Murante G., Springel V., Diaferio A., Dolag K., Moscardini L., Tormen G., Tornatore L., Tozzi P., 2004, MNRAS, 348, 1078
Byrd G., Valtonen M., 1990, ApJ, 350, 89
Castro-Rodríguez N., Aguerri J. A. L., Arnaboldi M., Gerhard O., Freeman K. C., Napolitano N. R., Capaccioli M., 2003, A&A, 405, 803
Cypriano E. S., Sodré L. J., Campusano L. E., Dale D. A., Hardy E., 2006, AJ, 131, 2417
D'Onghia E., Sommer-Larsen J., Romeo A. D., Burkert A., Pedersen K., Portinari L., Rasmussen J., 2005, ApJ, 630, L109
Eke V. R., Cole S., Frenk C. S., 1996, MNRAS, 282, 263
Feldmeier J. J., Ciardullo R., Jacoby G. H., Durrell P. R., 2003, ApJS, 145, 65
Feldmeier J. J., Ciardullo R., Jacoby G. H., Durrell P. R., 2004, ApJ, 615, 196
Feldmeier J. J., Mihos J. C., Durrell P. R., Ciardullo R., Jacoby G. H., 2003, in Kwok S., Dopita M., Sutherland R., eds, IAU Symposium Kinematics of Planetary Nebulae in M51's Tidal Tail. pp 633–+

Feldmeier J. J., Mihos J. C., Morrison H. L., Rodney S. A., Harding P., 2002, ApJ, 575, 779
Gal-Yam A., Maoz D., Guhathakurta P., Filippenko A. V., 2003, AJ, 125, 1087
Gerhard O., Arnaboldi M., Freeman K. C., Kashikawa N., Okamura S., Yasuda N., 2005, ApJ, 621, L93
Gnedin O. Y., 2003, ApJ, 589, 752
Gonzalez A. H., Zabludoff A. I., Zaritsky D., Dalcanton J. J., 2000, ApJ, 536, 561
Hernquist L., 1990, ApJ, 356, 359
Kauffmann G., 2001, in von Hippel T., Simpson C., Manset N., eds, ASP Conf. Ser. 245: Astrophysical Ages and Times Scales Formation Histories Expected From Cosmological Simulations. pp 381–+
Krick J. E., Bernstein R. A., Pimbblet K. A., 2006, AJ, 131, 168
Lin Y.-T., Mohr J. J., Stanford S. A., 2004, ApJ, 610, 745
Merritt D., 1984, ApJ, 276, 26
Merritt D., 1995, ArXiv Astrophysics e-prints
Mihos J. C., 2004, in Mulchaey J. S., Dressler A., Oemler A., eds, Clusters of Galaxies: Probes of Cosmological Structure and Galaxy Evolution Interactions and Mergers of Cluster Galaxies. pp 277–+
Mihos J. C., Harding P., Feldmeier J., Morrison H., 2005, ApJ, 631, L41
Monaco P., Fontanot F., Taffoni G., 2006, ArXiv Astrophysics e-prints
Monaco P., Murante G., Borgani S., Fontanot F., 2006, ApJ, 652, L89
Moore B., Katz N., Lake G., Dressler A., Oemler A., 1996, Nature, 379, 613
Murante G., Arnaboldi M., Gerhard O., Borgani S., Cheng L. M., Diaferio A., Dolag K., Moscardini L., Tormen G., Tornatore L., Tozzi P., 2004, ApJ, 607, L83
Napolitano N. R., Pannella M., Arnaboldi M., Gerhard O., Aguerri J. A. L., Freeman K. C., Capaccioli M., Ghigna S., Governato F., Quinn T., Stadel J., 2003, ApJ, 594, 172
Ostriker J. P., Hausman M. A., 1977, ApJ, 217, L125
Rudick C. S., Mihos J. C., McBride C., 2006, ApJ, 648, 936
Shen S., Mo H. J., White S. D. M., Blanton M. R., Kauffmann G., Voges W., Brinkmann J., Csabai I., 2003, MNRAS, 343, 978
Sommer-Larsen J., 2006, MNRAS, pp 509–+
Sommer-Larsen J., Romeo A. D., Portinari L., 2005, MNRAS, 357, 478
Springel V., 2005, MNRAS, 364, 1105
Springel V., Hernquist L., 2003, MNRAS, 339, 289
Springel V., White S. D. M., Tormen G., Kauffmann G., 2001, MNRAS, 328, 726
Springel V., Yoshida N., White S. D. M., 2001, New Astronomy, 6, 79
Stadel J. G., 2001, Ph.D. Thesis
Uson J. M., Boughn S. P., Kuhn J. R., 1991, ApJ, 369, 46
Wechsler R. H., Bullock J. S., Primack J. R., Kravtsov A. V., Dekel A., 2002, ApJ, 568, 52
Willman B., Governato F., Wadsley J., Quinn T., 2004, MNRAS, 355, 159
Zibetti S., White S. D. M., Schneider D. P., Brinkmann J., 2005, MNRAS, 358, 949

APPENDIX A: IDENTIFYING CLUSTER GALAXIES WITH SKID

For the purposes of the present work, we need a dynamical and automated way to identify galaxies in the simulations. Our galaxies must be self—bound structures, locally over-dense, and we need an operational procedure to unambiguously decide whether a star particle at a given redshift belongs to an object or not. For this reason, we follow the procedure adopted in M04 and use the publicly available SKID algorithm (Stadel 2001) and apply it to the distribution of star and dark matter particles.

The SKID algorithm works as follows:

- An overall density field is computed from the distribution of all available particle species, generally DM, gas and star particles. The density is estimated with a SPH spline–kernel, using a given number $N_{\rm sm}$ of neighbour particles. In the following we only include DM and star particles.
- The star particles are moved along the gradient of the density field in steps of $\tau/2$. When a particle begins to oscillate inside a sphere of radius $\tau/2$, it is stopped. In this way, τ can be interpreted as the typical size of the smallest resolved structure in the distribution of the star particles.
- When all star particles have been moved, they are grouped using a friends-of-friends (FOF) algorithm applied to the moved particle positions. The linking length is again $\tau/2$.
- The gravitational potential and binding energy of each group identified in this way is computed by accounting for all the particles inside a sphere centred on the centre of mass of the group and having radius 2τ (for the moved star particles, their initial positions are used in the computation of the potential). The binding energies of individual particles are then used to remove from the group all the star particles which are recognised as unbound, in an iterative way: the centre of mass of the group and its potential are recomputed after a particle has been discarded.
- Finally, we retain such a SKID–group of stars as a galaxy if it contains at least 32 particles after the removal of unbound stars. The exact value of this number threshold is unimportant, but the smaller the threshold is, the higher is the probability of identifying as "galaxy" a random set of neighbouring star particles. Using 32 particles correspond to a mass threshold of $M = 1.1 \times 10^{10} h^{-1} M_{\odot}$ for the cosmological simulation.

The resulting set of objects identified by SKID depends on the choice of two parameters, namely τ and $N_{\rm sm}$. After many experiments and resorting to visual inspection in a number of cases, we find that a complete detection of bound stellar objects requires the use of a set of different values of $N_{\rm sm}$. Using only one value for $N_{\rm sm}$ results in "missing" some galaxies. We use $N_{\rm sm} = 16, 32, 64$, and define a *galaxy* to be the set of star particles which belong to a SKID group for any one of the above $N_{\rm sm}$ values. If a star particle belongs to a SKID group for one value of $N_{\rm sm}$ and to another group for a different $N_{\rm sm}$, then the groups are joined and are considered as a single galaxy. All star particles not linked to any galaxies are considered to be part of the diffuse stellar component in the cluster. The left panel of Fig. 13 shows the surface density map of the DSC, as identified for our cluster D when all the three values of $N_{\rm sm}$ are used. In the right panel, we show the same map obtained using only $N_{\rm sm} = 32$. In the latter, the bright spots correspond to "missed" galaxies.

τ roughly corresponds to the size of the smallest resolved structure, and we adopt

$$\tau \approx 3\epsilon \qquad (A.1)$$

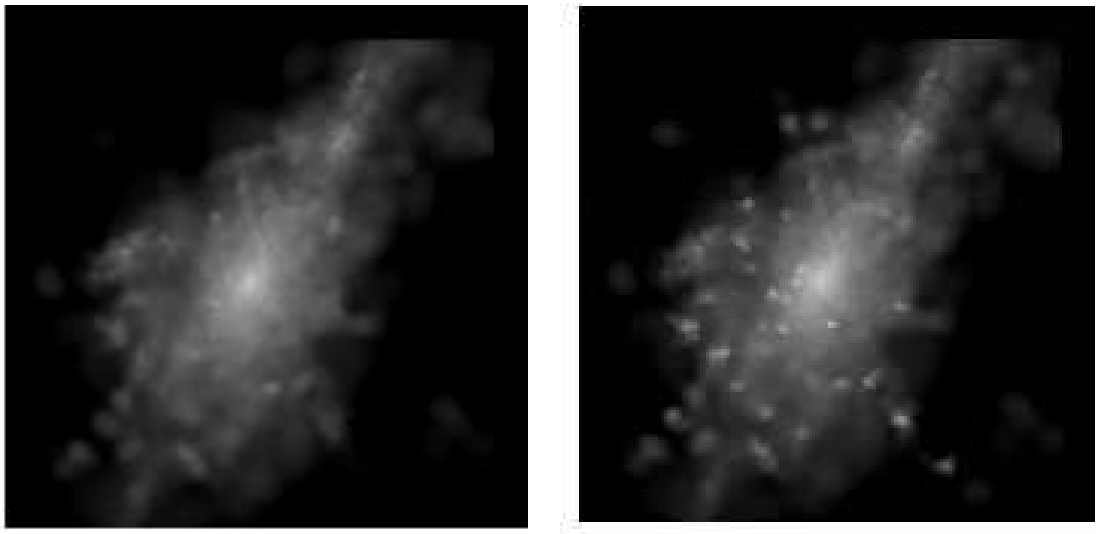

Figure 13. Surface density map of the DSC found in cluster D, when three values of $N_{\rm sm}$ are used (left panel) and when only one is used (right panel).

which is the scale where the softened force becomes equal to the Newtonian force. We have tested this choice by visual inspection in a number of clusters, and by performing an analysis of the velocity dispersions for the stars belonging to SKID galaxies and to the DSC. Fig. 14 shows the velocity dispersions for various components, namely the stars in galaxies, the stars in the DSC, the stars in the cD galaxy and the DM particles, for our cluster A (re-simulated at our higher resolution) when the value of τ is varied. The velocity dispersions are computed in spherical shells centred on the cluster centre, defined as the position of the DM particle having the minimum gravitational potential. For this high-resolution simulation, our fiducial choice is $\tau = 6h^{-1}$ kpc. In the bottom panel of Fig. 14, the spikes in the velocity distribution of the stars in galaxies (the solid curve) at $R > 100h^{-1}$ kpc correspond to SKID objects; no prominent spikes or bumps appear in the velocity dispersion profile for the DSC (long-dashed line), meaning that no structures in velocity that might correspond to "missed" galaxies are present in this component. Also, the value of the velocity dispersions for DSC and DM particles (dotted line) stay within ≈ 20 % from each other, as expected when both component sample the same gravitational cluster potential.

When a larger value is used ($\tau = 10h^{-1}$ kpc), spikes begins to appear in the DSC velocity dispersion curves, indicating that some objects, or part of them, are missed by the algorithm. This is especially clear for the spike at $R \approx 100h^{-1}$ kpc, which is present both in the velocity dispersion of stars in galaxies and in the velocity dispersion of the DSC, and clearly indicates that a fraction of stars in some galaxies have been mis-assigned to the diffuse component. Also, the discrepancy between DSC and DM velocity dispersions begins to grow, and the velocity dispersion of cD stars gets unrealistically large, $\sigma_v > 500$ km/s. This happens because some low–speed DSC stars begin to be assigned to the cD, whose typical star particle velocities are even lower, thus increasing the velocity dispersion of the cD star population. The situation gets worse it the value of τ is increased to $20h^{-1}$ kpc.

We have performed a similar analysis on some clusters taken from our cosmological set, where the fiducial value from eq. (A.1) is $\tau = 20h^{-1}$ kpc. Again, increasing τ to larger values results in having structures in the velocity space of the DSC, presumably due to missed objects. We conclude that the scaling (A.1) gives good results for the SKID galaxy identification, while keeping τ fixed to a given value (e.g. $20h^{-1}$ kpc) when the force resolution is varied is not a good choice.

When analysing particle distributions at redshift $z > 0$, we keep fixed the value of τ in co-moving coordinates, thus allowing the minimum physical size of our object to decrease with increasing redshift. While this does not obey equation (A1), τ never becomes less than ϵ. The effect is probably to slightly increase the amount of "volatile" galaxies at higher redshifts. Again, this choice was tested by visual inspection and by analysing the velocity dispersion distributions.

Also, we note that at high redshift ($z > 1$) the distribution of gas particles inside star–forming proto–clusters often contains adjacent clumps of star particles. Applying SKID to such distribution results in "galaxies" composed of two or more of such clumps, which instead should be considered as separate galaxies. For this reason, we choose to use only DM and star particles for the galaxy identification.

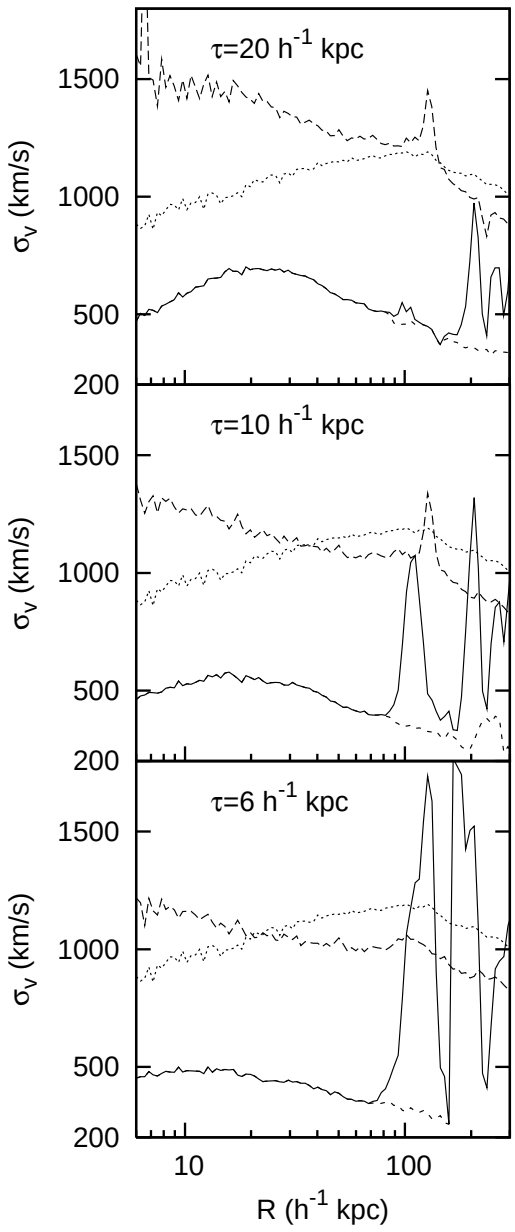

Figure 14. Velocity dispersions in the central part of cluster A, simulated at our higher resolution. Solid lines: stars belonging to SKID galaxies; long-dashed lines: DSC stars; dotted lines: DM particles; short-dashed lines: cD stars. Upper panel shows the results for the SKID analysis performed with a value of $\tau = 20h^{-1}$ kpc, centre panel for $\tau = 10h^{-1}$ kpc, lower panel for $\tau = 6h^{-1}$ kpc.